Inorganic Chemistry

ARTICLE

pubs.acs.org/IC

$VOPO_4 \cdot H_2O$: A Stacking Faults Structure Studied by X-ray Powder Diffraction and DFT-D Calculations

Romain Gautier, Nathalie Audebrand,* Eric Furet, Régis Gautier,* and Eric Le Fur*

Sciences Chimiques de Rennes, UMR 6226 CNRS, Université de Rennes 1-Ecole Nationale Supérieure de Chimie de Rennes, Avenue du Général Leclerc, CS 50837, 35708 Rennes Cedex 7, France

ABSTRACT: The dehydration process of $VOPO_4 \cdot 2H_2O$ occurs in two steps corresponding to successive elimination of the two crystallographically distinct water molecules. The intermediate phase $VOPO_4 \cdot H_2O$ has been stabilized for X-ray powder diffraction studies. The resulting data suggest a tetragonal cell (a = 6.2203(2) Å and c = 6.18867(7) Å), but an important anisotropy in the line broadening points out the necessity of considering a not perfectly organized structure. Because of the layered structure of this compound, density functional theory calculations including dispersion corrections have been carried out to evaluate the possible presence of stacking faults. The results of these calculations give information about the nature of the translations and their probabilities using a Boltzmann distribution. DIFFaX+ simulations of the X-ray powder diffraction pattern have been carried out using the results of the theoretical calculations and confirm the presence and nature of stacking faults.

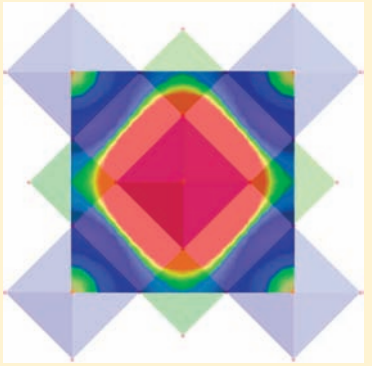

INTRODUCTION

Vanadium phosphate compounds are of great interest because of their catalytic properties. Indeed, they are actually used in industry for light hydrocarbon oxidation.[1] During the past few years, several studies have been devoted to various catalytic precursors in order to gain some information toward understanding their structural and catalytic behavior.[2−5] Among those precursors, the α form of $VOPO_4$,[6] denoted α_1-$VOPO_4$ according to Tachez,[7] was one of the first structurally characterized. This compound is known to be the main dehydration product of $VOPO_4 \cdot 2H_2O$. The latter is the most stable vanadium phosphate at room temperature.[8] Its crystallographic structure has been determined using X-ray powder diffraction within space group $P4/nmm$; the positions of hydrogen atoms could be determined using neutron powder diffraction on deuterated compounds.[9,10] α_1-$VOPO_4$ shows a lamellar crystallographic structure. Intercalation of mono- and divalent cations into the interlayer space is allowed by reduction of V(+V) to V(+IV). The structural, magnetic, thermal, and electrochemical properties of these intercalated vanadium phosphates have been largely studied.[11−13] Bordes et al. proposed a dehydration mechanism of $VOPO_4 \cdot 2H_2O$ that involves a monohydrate intermediate $VOPO_4 \cdot H_2O$.[14] The structure of the dihydrate compound is composed of two crystallographically independent water molecules: One is located in the interlayer space, while the other one lies in the vanadyl trans position. Assuming that this latter water molecule is more strongly bonded to the $VOPO_4$ sheets than the interlayer water molecules, the monohydrate structure has been supposed to be composed of $VOPO_4 \cdot H_2O$ layers without any water molecules located in the interlayer space. Bordes et al. proposed the $VOPO_4 \cdot H_2O$ structure to be tetragonal, space group $P4/nmm$, a = 6.21 Å, and c = 6.30 Å.[15]

The studies of several isostructural compounds of $AOBO_4 \cdot xH_2O$ formula with the A/B couple equal to V/P, V/As, V/Mo, V/S, Mo/P, Nb/P, Nb/As, Ta/P allowed a better understanding of the dehydration process of these layered compounds as well as intercalation of organic molecules within them.[12,16−18] In the dihydrate compounds, hydrogen bonds play an important role, as they are responsible for the layers cohesion. The lack of interlayer water molecules in the case of $VOPO_4 \cdot H_2O$ may therefore decrease the cohesion. The increase of $hk0$ line widths in the $VOPO_4 \cdot H_2O$ X-ray powder diagram that let us presume the occurrence of a slide of $VO(H_2O)PO_4$ layers support this assumption.

Although several papers deal with the hydration/dehydration process of $VOPO_4 \cdot 2H_2O$ using various techniques such as DSC, TGA, XRD, infrared, or Raman spectroscopies,[19−21] little structural information about hydrated vanadium phosphates $VOPO_4 \cdot nH_2O$ (n = 1 and n > 2) is available.[15,17,22] The present work aims to better characterize the $VOPO_4 \cdot H_2O$ structure using a new combined method to investigate stacking faults in layered compounds. To this end, density functional theory calculations including dispersion corrections (DFT-D) were combined with X-ray diffraction experiments for a better description of the possible slides of $VOPO_4 \cdot H_2O$ layers. DFT-D methods, which consists of adding a pairwise interatomic $C_6 R^{-6}$ term to the DFT energy, have proven to be accurate for a large range of chemical systems where noncovalent forces such as hydrogen-bonding and van der Waals interactions play a part.[23−28] DIFFaX+ refinements were carried out in order to describe the translation vectors and probabilities and the sequence of these stacking faults. This work allows a better understanding of the dehydration

Received: December 10, 2010
Published: April 21, 2011

process of hydrated vanadophosphates that plays an important part in the synthesis of vanadium phosphate catalysts. This is all the more significant because the catalytic properties of these compounds are strongly related to their structural properties.[1]

EXPERIMENTAL SECTION

Synthesis. The precursor $VOPO_4 \cdot 2H_2O$ has been prepared using a modified Ladwig method.[29] A 1.2 g amount of V_2O_5 was refluxed in a mixture of 10 mL of H_3PO_4 85%, 30 mL of H_2O, and 30 mL of HNO_3 65%. After 2 h, a yellow powder, identified by X-ray powder diffraction as $VOPO_4 \cdot 2H_2O$ (ICDD PDF 84-0111), was obtained. The product was washed with cold water and acetone.

Thermal Analyses. Thermogravimetric measurements were performed with a TGA 50 analyzer, Schimadzu. Differential scanning calorimetry was carried out on a TA Instruments Q10 under flowing N_2 (50 mL/min). Thermogravimetric analyses and differential scanning calorimetry were used with different heating rates. It allows appreciating precisely the temperature range of stabilization of this phase in order to optimize the thermodiffractometry experimental conditions.

X-ray Powder Diffraction. The high-resolution X-ray powder diagram used for studying the microstructure of $VOPO_4 \cdot H_2O$ has been recorded with a Bruker AXS D5005 powder diffractometer using a diffracted-beam-graphite monochromator (Cu $K\alpha_{1,2}$) and equipped with an Anton Paar HTK1200 oven camera. Partial dehydration of $VOPO_4 \cdot 2H_2O$ was carried out under flowing nitrogen at 30 °C, and the monohydrate phosphate was stabilized after cooling at room temperature under nitrogen. High-quality X-ray powder diffraction data for structure analysis were collected at 22 °C over the angular range 5−100° (2θ) with a counting time of 50 s step^{-1} and a step length of 0.02° (2θ).

X-ray Diffraction Line-Profile Analysis. For the microstructural analysis of $VOPO_4 \cdot H_2O$, instrumental line profiles for the Bruker D5005 diffractometer were obtained with the NIST standard reference material SRM660a LaB_6. For the whole pattern-fitting approach, the modeling of the instrumental profiles was carried out with the profile-fitting facility implemented in WinPLOTR.[30] Microstructure analysis was carried out from X-ray diffraction line-broadening analysis based on the whole pattern-fitting technique by means of the program FULLPROF.[31] In this approach, the integral breadths of the individual Bragg reflections are derived from a pseudo-Voigt approximation to separate apparent volume-weighted size and reticular distortions. Translation vectors and probabilities of stacking faults in $VOPO_4 \cdot H_2O$ were determined using DIFFaX+ code.[32] Within this code, the structure is described by stacking layers and the X-ray diffraction pattern is computed by integrating the intensities layer by layer.

Computational Details. DFT-D calculations were carried out using the CASTEP code.[33] The exchange and correlation potentials were calculated using the GGA in the parametrization of Perdew−Burke−Ernzerhof.[34] Dispersion corrections were added in the calculations within the scheme proposed by Tkatchenko and Scheffler.[35] Pseudopotentials were generated using the OTF_ultrasoftpseudo-potential generator included in the program. The electronic wave functions were sampled in the irreducible Brillouin zone (BZ) using the Monkhorst−Pack method.[36] All calculations were checked for convergence with respect to the kinetic energy cutoff of the plane waves basis set (up to 800 eV) and the *k*-points grid used for integration over the BZ. Geometry optimizations were carried out without any symmetry constraints; only cell angles were fixed to 90°.

RESULTS

Thermal Analyses. Thermal analyses show two steps of dehydration with enthalpies of decomposition of 110 and 167.3 J·g^{-1} corresponding to loss of the two H_2O molecules.

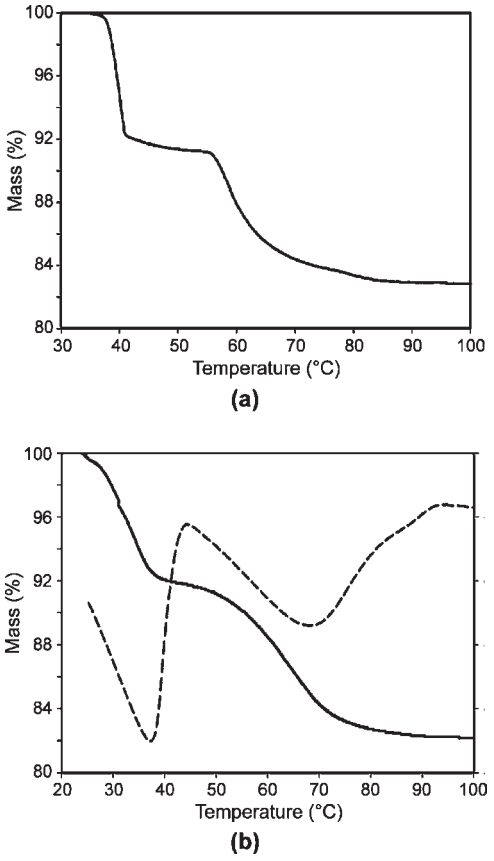

Figure 1. Thermogravimetric (plain) and DSC (dotted) analyses of $VOPO_4 \cdot 2H_2O$ dehydration under humid N_2 (a) and under dry N_2 (b).

Analyses with a heating rate of 0.2 °C/min under humid N_2 flux (50 mL/min) allow one to isolate the monohydrate between 45 and 55 °C (Figure 1a). Using dry N_2 flux (50 mL/min), the temperature range of isolation depends upon the heating rate. Figure 1b shows TG and DSC analysis of $VOPO_4 \cdot 2H_2O$ with a heating rate of 0.1 °C/min in dry N_2 flux. The two-step dehydration was also observed at 30 °C in dry N_2 flux and allows isolation of the monohydrate during X-ray diffraction.

X-ray Powder Diffraction. X-ray thermodiffractometry suggests that the partially dehydrated compound keeps its lamellar aspect but the interlayer distance *c* is reduced from 7.410(1)[9] to 6.18867(7) Å (a = 6.22027(20) Å). The powder data exhibit an important anisotropy in line broadening (Figure 2). The single lines were fitted using the WinPLOTR software. Gaussian and Lorentzian parts of each single line were extracted and deconvoluted from the instrumental contribution, leading to intrinsic integral breadth.[37] A Williamson−Hall plot has been drawn (Figure 3). Reflection 321 has been omitted because of an important measurement uncertainty that is due to its very low intensity.

From the variation of the reciprocal integral breadth as a function of the reciprocal intereticular distance, the line-broadening anisotropy is confirmed. Indexing of the diffraction lines is quite ambiguous since multiple indexings are possible due to close *a* and *c* unit-cell parameters. Nevertheless, the plot could be interpreted in that way: it evidenced a very low amount of reticular distortions and anisotropic crystallites with an average cylindrical shape with a height higher than the diameter, which could be in agreement with the tetragonal symmetry. No stacking faults could be evidenced at this stage.

dx.doi.org/10.1021/ic102473s |*Inorg. Chem.* 2011, 50, 4378–4383

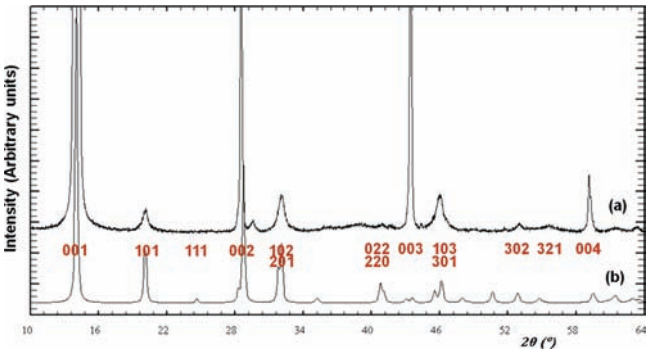

Figure 2. (a) Experimental X-ray diffraction pattern of $VOPO_4 \cdot H_2O$ (a) and simulated X-ray diffraction pattern of a well-ordered $VOPO_4 \cdot H_2O$ model (b).

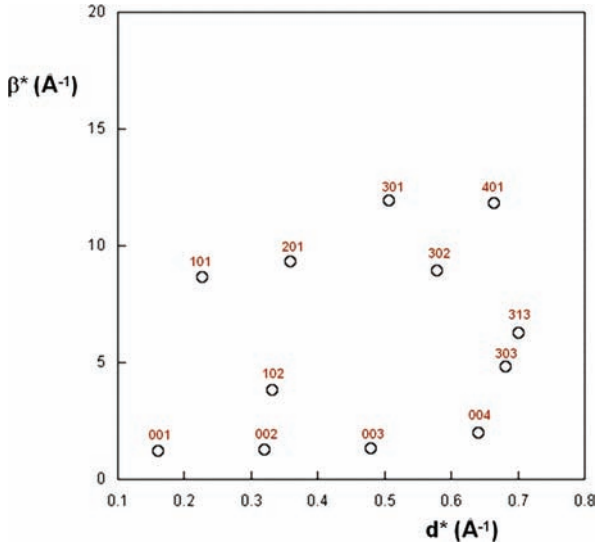

Figure 3. Williamson–Hall plot of $VOPO_4 \cdot H_2O$.

In the pattern matching the Thompson–Cox–Hastings pseudo-Voigt function was selected to approximate the observed line profiles. The background was described with a linear interpolation between refined intensity points. The refinement involved the following parameters: one zero-point, two unit-cell parameters, two line asymmetry parameters, five parameters for the description of the background, and three crystallite size parameters in a platelet-like model. The final refinement converged to the residual factors $R_P = 0.16$ and $R_{WP} = 0.23$. The results were derived for isotropic line broadening with 46.0 and 21.5 nm for the apparent crystallite height and diameter, respectively, in agreement with a mean cylindrical shape, and no residual strains. This calculated cylindrical shape disagrees with previous experimental observations, suggesting thin plate morphology of the crystallites.[22]

DFT-D Calculations. First-principles calculations were carried out in order to study gliding properties of $VOPO_4 \cdot H_2O$ layers that may be at the origin of the line broadening of X-ray diffraction data. Layer rotations were not considered due to important steric repulsions. As shown by infrared experiments,[19] the coordinated water molecule in $VOPO_4 \cdot H_2O$ is the one located in the trans position to the vanadyl bond. Therefore, the monohydrate layer of $VOPO_4 \cdot 2H_2O$ has been used as a starting point to model the monohydrate layer. Geometry optimization of an isolated monohydrate layer was first done. Such a layer has been considered in an orthorhombic supercell with a *c* parameter equal to 12 Å that prevents interaction between layers. Among the cell parameters, only *a* and *b* parameters were allowed to relax during optimization. Although no symmetry constraints were considered, no distortion of $VOPO_4 \cdot H_2O$ occurs during optimization. The small difference between *a*- and *b*-optimized parameters that is equal to 6.251 and 6.229 Å, respectively, results from the hydrogen atoms of the water molecules that slightly lower the tetragonal symmetry. The overall optimized bond distances sketched in Table 1 compare well with the corresponding ones in $VOPO_4 \cdot 2H_2O$.[9,10] For instance, the vanadyl bond that is the shortest V–O distance is equal to 1.576 and 1.570 Å for $VOPO_4 \cdot 2H_2O$ and optimized monohydrate layer $VOPO_4 \cdot H_2O$, respectively. The unique significant difference occurs for the contact between the vanadium atoms and the water molecules. The optimized $V-OH_2$ distance is computed to be longer by ca. 0.17 Å than the corresponding one in the crystal structure of $VOPO_4 \cdot 2H_2O$. However, the potential energy curve of this weak bond is almost flat in the range between 2.20 and 2.50 Å. In order to evaluate the bonding energy between the oxygen atom of the water molecule and the vanadium atom, total energy has been computed for monohydrate layers whose $V-OH_2$ distance has been gradually lengthened until total energy reached a nearly constant value. The resulting bonding energy is estimated around 8 kcal·mol^{-1}. Such a value is of the same order of magnitude as hydrogen bonds that must occur in $VOPO_4 \cdot 2H_2O$ for the free water molecules. This explains why both dehydration enthalpies are close in energy.

In order to study the disorder along the *c* axis in the $VOPO_4 \cdot H_2O$ layer, energy calculations were monitored with different interlayer distances and translations. Orthogonal supercells

Table 1. Selected Interatomic Experimental and Optimized Distances of $VOPO_4 \cdot nH_2O$ ($n = 1, 2$)

	$VOPO_4 \cdot 2H_2O$, *P*4/*nmm*, single-crystal diffraction[9]	$VOPO_4 \cdot H_2O$, *P*1, DFT-D optimized
V–O (Å)	1.5665(52)	1.576
	1.9080(25) (×4)	1.898 (×2) – 1.918 (×2)
	2.2334(52)	2.405
P–O (Å)	1.5319(24) (×4)	1.537 (×2) – 1.543 (×2)
O–H (Å)		0.974

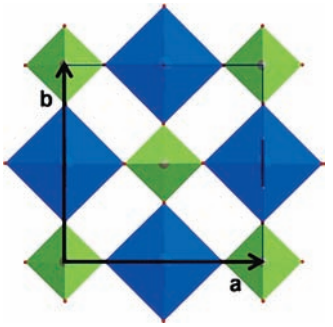

Figure 4. View of a $VOPO_4 \cdot H_2O$ layer. Green tetrahedra and blue octahedra are coordination polyhedra of P and V atoms, respectively.

dx.doi.org/10.1021/ic102473s |*Inorg. Chem.* 2011, 50, 4378–4383

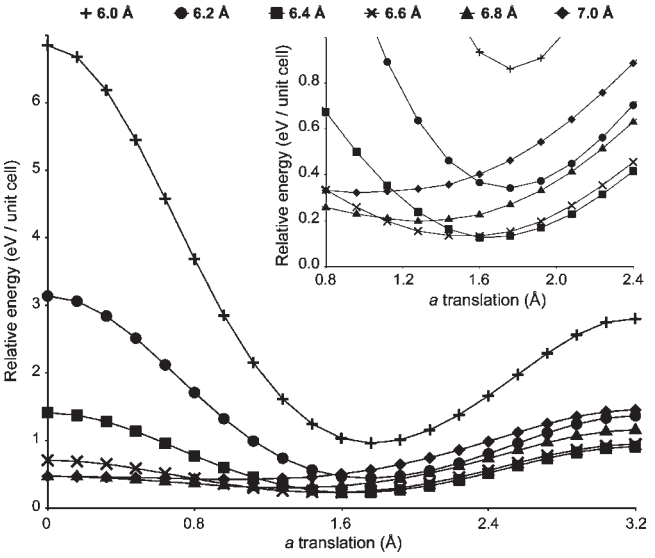

Figure 5. Energy calculations of translation along the *a* axis. The inset is a zoomed picture around the minimum energy.

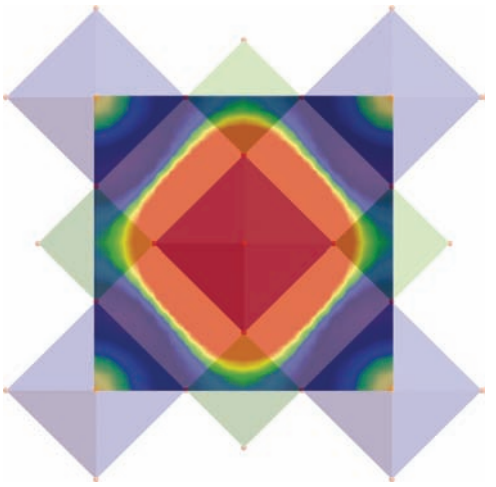

Figure 6. Energy vs layer-to-layer translation along *a* and *b* relative to the $VOPO_4 \cdot H_2O$ structure for an interlayer distance of 6.2 Å. Red and dark blue regions correspond to the highest and lowest energies, respectively.

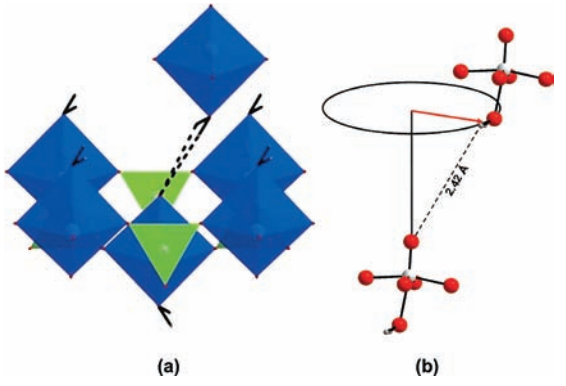

Figure 7. Description of hydrogen bonding in the $VOPO_4 \cdot H_2O$ structure. V, O, and H atoms are large white, large red, and small gray spheres, respectively; green tetrahedra and blue octahedra are coordination polyhedra of P and V atoms, respectively.

containing two layers have been considered to model the stacking faults. The optimized values of *a* and *b* cell parameters have been used. Calculations describing *a* and *b* gradual translations were carried out for *c* parameters ranging from 6 to 7 Å (Figure 5). Owing to the symmetry of the layer, translations along the *a* and *b* axes only differ by the positions of H atoms of the water molecules. Thus, as foreseen, computed energy curves are very similar, whatever the translation is done along *a* or *b*. Therefore, only the curve for *a* translations is sketched in Figure 5. According to Figure 5, energy minima are obtained for a translation of about 1.7 ± 0.1 Å in *a* directions whatever the *c* parameter value. The energetic gain in comparison with the well-ordered structure is significant for *c* parameters lower or equal than 6.6 Å. This disagrees with the assumption of Bordes et al.[15] Starting from $VOPO_4 \cdot 2H_2O$, when the water molecule that is not coordinated to the vanadium atom is moving off the structure, the interlayer distance is reduced from 7.41 to 6.19 Å. The distance between the O atom of the vanadyl bond and the H_2O molecule of the upper layer is equal to 2.14 Å, which entails increasing repulsion and inducing a shift of one layer with respect to neighboring ones. In order to get a refined description, the scanning area $[a/2, b/2]$ of layer to layer translations with $a/20$ and $b/20$ steps has been explored for an interlayer distance of 6.2 Å that is very close to the refined parameter. Total energy surface is sketched in Figure 6. This shows that translations of about 1.7 Å of consecutive layers stabilize the structure whatever their directions. $a + b$ translations greater than 1.8 Å are not favored because of the repulsion between the H_2O molecules of two neighboring layers.

DISCUSSION

Since its first isolation,[14] the $VOPO_4 \cdot H_2O$ structure had not been determined. The only structural information available from X-ray diffraction is that the interlayer distance is equal to 6.19 Å. Considering the space group *P*4/*nmm* that is one of the dihydrate and the anhydrous vanadium phosphate α_1-$VOPO_4$, the structure could not be successfully determined. The X-ray diffraction line-profile analysis allows us to provide clues concerning the crystallite size. This results in a cylindrical shape of the monohydrate crystallite. Stacking faults can contribute to the apparent crystallite size. The broadening of (00*l*) reflections is not significant compared to other reflections. This suggests that the interlayer distance can be considered constant whatever the stacking faults. This differs from others layered compounds like trigonal $Ni(OH)_2$ where the interlayer distance can vary according to the considered stacking.[38]

The interlayer distance may be controlled by hydrogen bonds between the H_2O located trans to the vanadyl bond and the V═O of the closest layer (Figure 7a). The favored displacement of 1.7 Å of the layers from one to another leads to distances of ~2.4 Å between the oxygen atom of the vanadyl bond and the hydrogen atoms of the neighboring layer water molecules (Figure 7b). This distance is consistent with the occurrence of significant hydrogen bonds.

In order to study stacking faults, several programs such as DIFFaX,[39] DIFFaX+,[32] and FAULTS[40] can take into account translations vectors and their probabilities for simulation of X-ray diffraction patterns. In particular, DIFFaX+ allows refinement of translation vectors.[41] If no translation between neighboring layers

dx.doi.org/10.1021/ic102473s |*Inorg. Chem.* 2011, 50, 4378–4383

Table 2. Information of the Different Stacking Faults and Their Probabilities Refined by DIFFaX+ Code

transition description	stacking vectors	refined probabilities
1 to 1	(0, 0.275)	0.18
1 to 2	(0, −0.275)	0.79
1 to 3	(0.275, 0)	0.00
1 to 4	(−0.275, 0)	0.03
2 to 1	(0, 0.275)	1.00
2 to 2	(0, −0.275)	0.00
2 to 3	(0.275, 0)	0.00
2 to 4	(−0.275, 0)	0.00
3 to 1	(0, 0.275)	0.01
3 to 2	(0, −0.275)	0.00
3 to 3	(0.275, 0)	0.04
3 to 4	(−0.275, 0)	0.95
4 to 1	(0, 0.275)	0.99
4 to 2	(0, −0.275)	0.00
4 to 3	(0.275, 0)	0.01
4 to 4	(−0.275, 0)	0.00

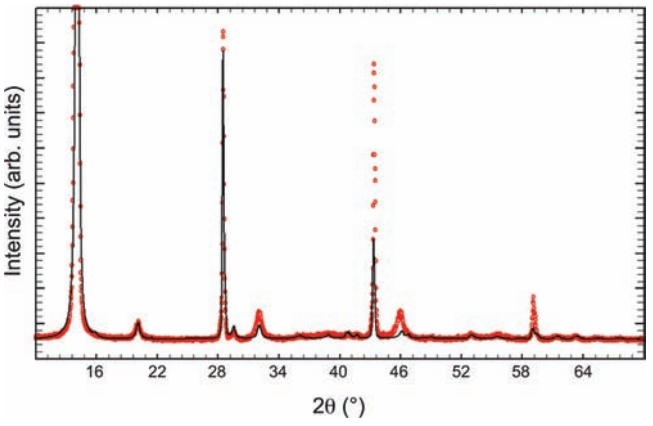

Figure 8. Comparison between refined powder pattern (black) and experimental (red) X-ray diffraction pattern (see text for details).

is considered, there is a large discrepancy between the calculated and the simulated X-ray diffraction pattern (R_{wp} = 26.38%, R_{exp} = 5.32%). The four translations (0, 0.275), (0, −0.275), (0.275, 0), and (−0.275, 0) have been taken into account in the simulation. They correspond to the most stable configurations identified by DFT-D calculations. Because those calculations do not consider full relaxation of the atomic positions, additional DFT-D calculations have been carried out in order to confirm the energy surface. Structures that take into account the (0, 0.275) and (0.275, 0) translations, i.e., when neighboring layers are translated of 1.70 Å in each case, have been computed to be more stable by only 0.3 eV per $VOPO_4$ unit with respect to the one without any translation. Crystal structures with those translations are very close in energy and differ solely by the hydrogen-bond network. Computed energies were used to estimate probabilities of translation along some directions using the Boltzmann distribution. Different stacking fault sequences were also considered. The layer-to-layer transition probabilities were refined in order to obtain the best fit between experimental and simulated X-ray diffraction patterns. Considering a simple model with the four equivalent translations without any specific sequence, that is, no refinement of their probabilities, does not improve the fit between calculated and simulated X-ray diffraction patterns. If, however, the four equivalent translations are considered within the 16 sequences given in Table 2, refinement of probabilities allows a significant improvement of the agreement factors (R_{wp} = 18.40%, R_{exp} = 5.32%) as shown in Figure 8. By considering specific sequences, it is also possible to improve these factors. In this case, because of the high probability of transitions 1 to 2 and 2 to 1, the most probable transition sequence is −1−2−1−2−1−2−. Moreover, it should be pointed out that the agreement factors have not be further improved considering models with additional layer translation vectors.

CONCLUSION

Oxovanadium phosphate compounds have attracted much interest in the physical and chemical communities because of their participation as constituents or precursors of the active phase in an efficient industrial catalyst. Because many phases can play a part in the catalytic process, especially $VOPO_4$, it is of great interest to learn about their structural properties. Since $VOPO_4 \cdot H_2O$ is an intermediate compound that can be observed during the dehydration of $VOPO_4 \cdot 2H_2O$ to $VOPO_4$, knowledge of this monohydrate can help in understanding the structural properties of these phases, which is still a matter of debate.[1]

This study is based on the combined use of first-principles calculations and X-ray powder diffraction techniques. DFT-D calculations showed that a translation of 1.70 Å between two stacked layers stabilizes the crystal structure. This information was further used in DIFFaX+ program in order to describe the complex disorder of these layers and simulate X-ray diffraction pattern. In spite of the difficulties to collect a high-quality X-ray diffraction pattern for the monohydrate, refinement of translation probabilities was able to give a much better description of the translations and improve the agreement between experimental and simulated diffraction patterns.

The $VOPO_4 \cdot H_2O$ layered compound is shown to be a not well-ordered compound, and translations of 1.7 Å in every direction have to be considered to avoid important repulsions between layers. Hydrogen bonds between layers allow keeping the same interlayer distance whatever the translation considered. Anhydrous structures are therefore probably governed by the presence of stacking faults within the monohydrate phase. This could explain why the structural model given in the literature for the dehydrated compound is not in good agreement with the experimental data.

AUTHOR INFORMATION

Corresponding Author

*E-mail: nathalie.audebrand@univ-rennes1.fr (N.A.), regis.gautier@ensc-rennes.fr (R.G.), eric.le-fur@ensc-rennes.fr (E.L.F.).

ACKNOWLEDGMENT

This work was granted access to the HPC resources of CINES under the allocation 2009-[scr6170] made by GENCI (Grand Equipement National de Calcul Intensif).

REFERENCES

(1) Conte, M.; Budroni, G.; Bartley, J. K.; Taylor, S.; Carley, A. F.; Schmidt, A.; Murphy, D. M.; Girgsdies, F.; Ressler, T.; Schlögl, R.; Hutchings, G. J. *Science* **2006**, *313*, 1270.

(2) Hutchings, G. J.; Sananes, M. T.; Sajip, S.; Kiely, C. J.; Burrows, A.; Ellison, I. J.; Volta, J. C. *Catal. Today* **1997**, *33*, 161.
(3) Bartley, J. K.; Lopez-Sanchez, J. K.; Hutchings, G. J. *Catal. Today* **2003**, *81*, 197.
(4) Griesel, L.; Bartley, J. K. W. R. P. K.; Hutchings, G. J. *J. Mol. Catal. A: Chem.* **2004**, *220*, 113.
(5) Ryumon, N.; Imai, H. K. Y.; Okuhara, T. *Appl. Catal. A: Gen.* **2006**, *297*, 73.
(6) Jordan, B. D.; Calvo, C. *Can. J. Chem.* **1973**, *51*, 2621.
(7) Tachez, M.; Theobald, F.; Bordes, E. *J. Solid State Chem.* **1981**, *40*, 280.
(8) Ben Abdelouahab, F.; Volta, J. C.; Olier, R. *J. Catal.* **1994**, *148*, 334.
(9) Tietze, H. R. *Aust. J. Chem.* **1981**, *34*, 2035.
(10) Tachez, M.; Theobald, F.; Bernard, J.; Hewat, A. W. *Rev. Chim. Min.* **1982**, *19*, 291.
(11) Melánová, K.; Votinský, J.; Beneš, L.; Zima, V. *Mater. Res. Bull.* **1995**, *30*, 1115.
(12) Kalousová, J.; Votinský, J.; Beneš, L.; Melánová, K.; Zima, V. *Collect. Czech. Chem. Commun.* **1998**, 63.
(13) Beneš, L.; Melánová, K.; Trchová, M.; Čapková, P.; Matějka, P. *Eur. J. Inorg. Chem.* **1999**, 2289.
(14) Bordes, E.; Courtine, P.; Pannetier, G. *Ann. Chim. Paris* **1973**, *8*, 105.
(15) Bordes, E. *Catal. Today* **1987**, *1*, 499.
(16) Johnson, J. W.; Jacobson, A. J.; Brody, J. F.; Rich, S. M. *Inorg. Chem.* **1982**, *21*, 10.
(17) Beneke, K.; Lagaly, G. *Inorg. Chem.* **1983**, *22*, 10.
(18) Kasthuri Rangan, K.; Gopalakrishnan, J. *Inorg. Chem.* **1996**, *35*, 6080.
(19) Trchová, M.; Čapková, P.; Matějka, P.; Melánová, K.; Beneš, L.; Uhlířová, E. *J. Solid State Chem.* **1999**, *148*, 197.
(20) Beneš, L.; Černošková, E.; Malek, J.; Melánová, K.; Patrono, P.; Zima, V. *J. Inclusion Phenom. Macrocyclic Chem.* **2000**, *36*, 163.
(21) Beneš, L.; Melánová, K.; Zima, V.; Trchová, M.; Uhlířová, E.; Matějka, P. *Eur. J. Inorg. Chem.* **2000**, 895.
(22) R' Kha, C.; Vandenborre, M. T.; Livage, J.; Prost, R.; Huard, E. *J. Solid State Chem.* **1986**, *63*, 202.
(23) Grimme, S. *J. Comput. Chem.* **2004**, *25*, 1463.
(24) Grimme, S. *J. Comput. Chem.* **2006**, *27*, 1787.
(25) Jurecka, P.; Cerný, J.; Hobza, P.; Salahub, D. *J. Comput. Chem.* **2007**, *28*, 555.
(26) Barone, V.; Biczysko, M.; Pavone, M. *Chem. Phys.* **2008**, *346*, 247.
(27) Grimme, S.; Antony, J.; Ehrlich, S.; Krieg, H. *J. Chem. Phys.* **2010**, *132*, 154104.
(28) Thanthiriwatte, K. S.; Hohenstein, E. G.; Burns, L. A.; Sherrill, C. D. *J. Chem. Theory Comput* **2011**, *7*, 88.
(29) Ladwig, G. *Z. Anorg. Allg. Chem.* **1965**, *338*, 266.
(30) Roisnel, T.; Rodriguez-Carvajal, J. *Mater. Sci. Forum* **2001**, *378*−*381*, 118.
(31) Rodriguez-Carvajal, J.; Roisnel, T. *Mater. Sci. Forum* **2002**, *443*−*444*, 123.
(32) Leoni, M.; Gualtieri, A. F.; Roveri, N. *J. Appl. Crystallogr.* **2004**, *37*, 166.
(33) Seagall, M. D.; Lindan, P. J. D.; Probert, M. J.; Pickard, C. J.; Hasnip, P. J.; Clark, S. J.; Payne, M. C. *J. Phys.: Condens. Matter* **2002**, *14*, 2717.
(34) Perdew, J. P.; Burke, S.; Ernzerhof, M. *Phys. Rev. Lett.* **1996**, *77*, 3865.
(35) Tkatchenko, A.; Scheffler, M. *Phys. Rev. Lett.* **2009**, *102*, 073005.
(36) Monkhorst, H. J.; Pack, J. D. *Phys. Rev. B* **1976**, *13*, 5188.
(37) Stokes, A. R. *Proc. Phys. Soc. London* **1948**, 61.
(38) Delmas, C.; Tessier, C. *J. Mater. Chem.* **1997**, *7*, 1439.
(39) Treacy, M. M. J.; Newsam, J. M.; Deem, M. W. *Proc. R. Soc. London, Ser. A* **1991**, *433*, 499.
(40) Casas-Cabanas, M.; Palacin, M. R.; Rodriguez-Carvajal, J. *Z. Krist. Suppl.* **2006**, *23*, 243.
(41) See for example Johnsen, R. E.; Norby, P. *J. Phys. Chem. C* **2009**, *113*, 19061.